JOC Article
pubs.acs.org/joc

Nondoped Pure-Blue OLEDs Based on Amorphous Phenylenevinylene-Functionalized Twisted Bimesitylenes

Jarugu Narasimha Moorthy,*,† Parthasarathy Venkatakrishnan,† Palani Natarajan,† Zhenghuan Lin,‡ and Tahsin J. Chow*,‡

†Department of Chemistry, Indian Institute of Technology, Kanpur 208016, India, and ‡Institute of Chemistry, Academia Sinica, Taipei, Taiwan 115, Republic of China

moorthy@iitk.ac.in; tjchow@chem.sinica.edu.tw

Received January 29, 2010

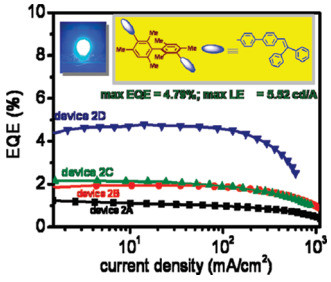

The twisted bimesitylene scaffold hinders crystallization and imparts amorphous nature to the oligophenylenevinylenes (OPVs) generated by 2- and/or 4-fold functionalization. The resultant phenylenevinylenes **1**−**5** with unique molecular topology exhibit excellent thermal and solid-state luminescence properties. The amorphous nature permits their application as pure-blue emissive materials in OLEDs. Under nondoped conditions, the device performances observed surpass those for analogous and simple oligophenylenevinylenes known so far; for example, the device based on OPV **2** as an emitting material and structurally analogous **Bim-DPAB** as a hole-transporting material yields pure-blue electroluminescence with an external quantum efficiency of ca. 4.70% at 20 mA/cm^2, which is higher than those reported for nondoped pure-blue OPV emitters.

1. Introduction

The organic π-conjugated systems based on polyphenylenevinylenes (PPV) and oligophenylenevinylenes (OPV) are of immense interest at the present time due to their applications in light-emitting diodes (LEDs), semiconducting and photoconducting devices, nonlinear optics, light-harvesting antennas, etc.[1] Insofar as organic LEDs are concerned, OPVs constitute excellent materials for light emission.[2] However, a serious drawback, as exemplified by the representative distyrylbenzene (DSB) and its derivatives, is that the fluorescence in the solid state is efficiently quenched, while emission occurs in the solution state with a very high efficiency.[3] The quenching in the solid state has been attributed to intermolecular $\pi-\pi$ stacking interactions and H-type aggregation, which lead to the formation of excimers.[4] Thus, various strategies have been explored to obviate quenching in the solid state and increase photoluminescence efficiency via suppression of molecular aggregation. The tetrahedrally linked DSBs, viz. tetrakis(4-*tert*-butylstyrylstilbenyl)methane C(^{t}BuSSB)$_4$[5a] and tetrakis(4-(4′-(3″,5″-dihexyloxystyryl)styryl)stilbenyl)methane

(1) (a) Lakowicz, J. R. *Principles of Fluorescence Spectroscopy*, Plenum Press: New York, 1999. (b) Meier, H. *Angew. Chem., Int. Ed. Engl.* **1992**, *31*, 1399. (c) Tessler, N.; Denton, G. J.; Friend, R. H. *Nature* **1996**, *382*, 695. (d) Tour, J. M. *Chem. Rev.* **1996**, *96*, 537. (e) Kraft, A.; Grimsdale, A. C.; Holmes, A. B. *Angew. Chem., Int. Ed.* **1998**, *37*, 402. (f) *Organic Electroluminescence*; Kafafi, Z. H., Ed.; Taylor and Francis: Boca Raton, FL, 2005; Optical Engineering Vol. 94. (g) *Organic Light Emitting Devices. Synthesis, Properties and Electronic Applications*; Mullen, K., Scherf, U., Eds.; Wiley: Weinheim, Germany, 2006.

(2) (a) *Electronic Materials: The Oligomer Approach*; Müllen, K., Ed.; Wiley-VCH: Weinheim, Germany, 1998. (b) Liu, B.; Bazan, G. C. *Organic Electroluminescence*; Kafafi, Z. H., Ed.; Taylor and Francis: Boca Raton, FL, 2005; Optical Engineering Vol. 94.

(3) (a) Oelkrug, D.; Tompert, A.; Egelhaaf, H.-J.; Hanack, M.; Steinhuber, E.; Hohloch, M.; Meier, H.; Stalmach, U. *Synth. Met.* **1996**, *83*, 231. (b) Oelkrug, D.; Tompert, A.; Gierschner, J.; Egelhaaf, H.-J.; Hanack, M.; Hohloch, M.; Steinhuber, E. *J. Phys. Chem. B* **1998**, *102*, 1902. (c) Ruiz, P. M.; Behnisch, B.; Schweikart, K. H.; Hanack, M.; Ler, L.; Oelkrug, D. *Chem.—Eur. J.* **2000**, *6*, 1294.

(4) Würthner, F.; Thalacker, C.; Dieke, S.; Tschierske, C. *Chem.—Eur. J.* **2001**, *7*, 2245.

(5) (a) Wang, S.; Oldham, W. J. Jr.; Hudack, R. A. Jr.; Bazan, G. C. *J. Am. Chem. Soc.* **2000**, *122*, 5695. (b) Robinson, M. R.; Wang, S.; Bazan, G. C.; Cao, Y. *Adv. Mater.* **2000**, *12*, 1701. (c) Gu, T.; Accorsi, G.; Armaroli, N.; Guillon, D.; Nierengarten, J. F. *Tetrahedron Lett.* **2001**, *42*, 2309.

DOI: 10.1021/jo1001565 Published on Web 03/23/2010
© 2010 American Chemical Society

CHART 1. Structures of the OPVs 1−5

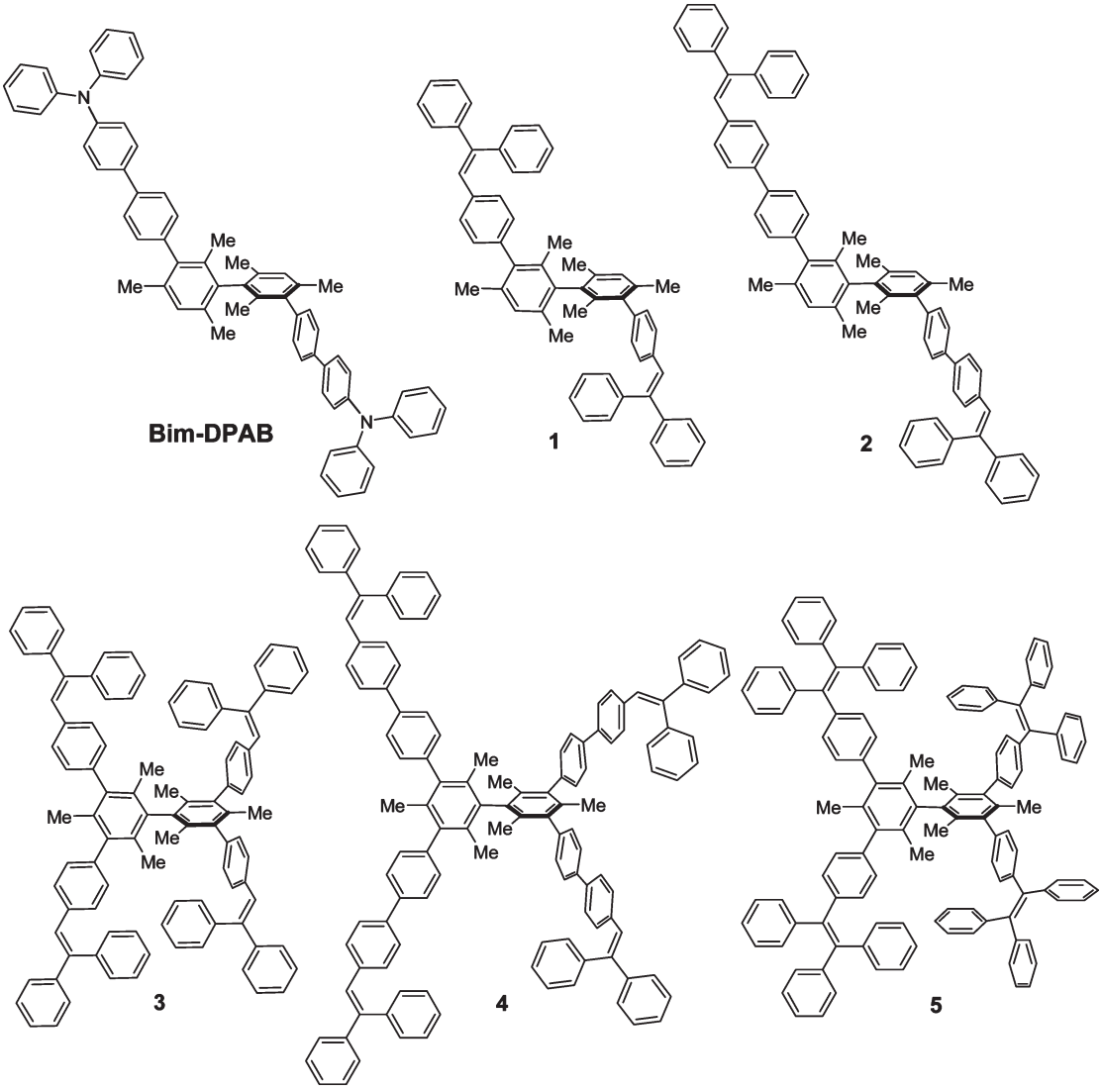

T-4R-C_6H_{13},[5b] and 4-fold DSB-functionalized calix[4]arenes[5c] are some examples of rational approaches aimed at enhancing the emission in the solid state. Incidentally, the device performances with such molecular systems are not entirely encouraging.[5a,b] A classical blue-emitting dopant such as 4,4′-bis(2,2-diphenylvinyl)biphenyl (DPVBi) has been found to exhibit bluish-green electroluminescence based on color chromaticity diagram in addition to the fact that its glass transition temperature (T_g) is not appreciably high (below 100 °C).[6] Indeed, OPVs that exhibit pure-blue emission with a high EL efficiency, brightness, and stability are still rare.

We have recently shown that the twisted anthracene-functionalized bimesitylenes exhibit amorphous behavior and that they can be exploited as brilliant emitting materials for application in LEDs.[7a] We have also demonstrated the utility of diarylamino end-capped bimesitylenes (e.g., **Bim-DPAB** in Chart 1) as emitting as well as hole-transporting materials in organic LEDs.[7b] In continuation of these studies, we surmised that the twisted bimesityl core can be beneficially exploited to develop OPVs with better optical properties and high T_g values. Thus, we designed 2- and 4-fold OPVs **1**−**5** in Chart 1 with the following rationale:

- the "twisted" geometry introduced by the bimesityl core supposedly hinders close packing of molecules, leading to amorphous property,[8] which is essential for application as materials in OLEDs.
- the difficulty associated with the close packing of three-dimensional molecules with orthogonal planes typified by bimesityl presumably suppresses the self-quenching, such that the emission quantum yields are enhanced in the solid state as compared to those in the solution state.
- the unique molecular topology with *meta* linkage restricts the conjugation and hence conserves the optical properties of the chromophoric units that are attached to the core.

(6) Matsurra, M.; Kusumoto, T.; Tokailin, H. US Patent 5 516 577, **1996**.
(7) (a) Moorthy, J. N.; Venkatakrishnan, P.; Natarajan, P.; Huang, D.-F.; Chow, T. J. *J. Am. Chem. Soc.* **2008**, *130*, 17320. (b) Moorthy, J. N.; Venkatakrishnan, P.; Huang, D.-F.; Chow, T. J. *Chem. Commun.* **2008**, 2146.
(8) (a) Shirota, Y. *Organic Electroluminescence*; Kafafi, Z. H., Ed.; Taylor and Francis: Boca Raton, FL, 2005; Optical Engineering Vol. 94, Chapter 4, p 147. (b) Shirota, Y. *J. Mater. Chem.* **2005**, *15*, 75. (c) Shirota, Y.; Kageyama, H. *Chem. Rev.* **2007**, *107*, 953.

SCHEME 1. Synthesis of OPVs 1−5[a]

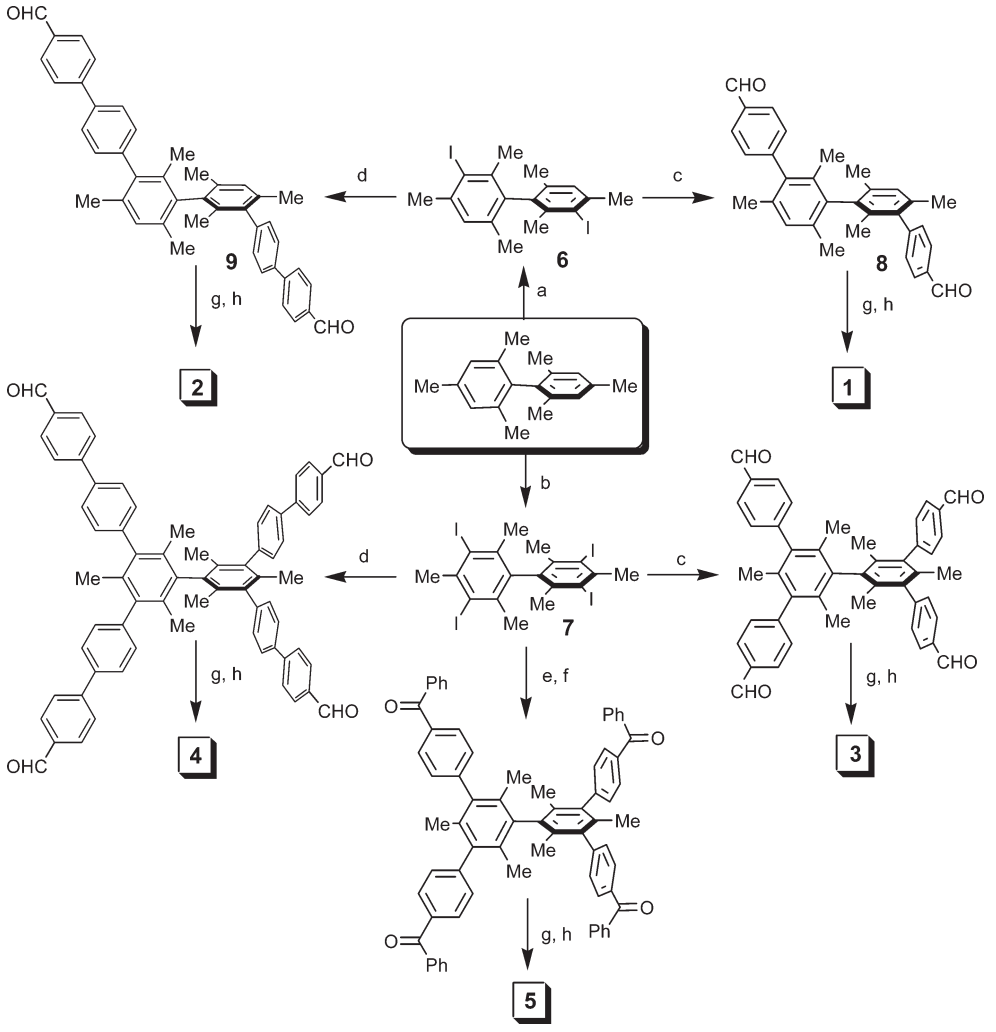

[a]Reagents and conditions: (a) NIS, TFA (catalytic amount), CH_3CN, 5 °C to rt, 8 h, 83%; (b) I_2, HNO_3/H_2SO_4 (1:1), $CHCl_3$, AcOH, 0 °C to rt, 3 h, 86%; (c) 4-formylphenylboronic acid, $Pd(PPh_3)_4$, 2 M K_2CO_3, toluene/THF (2:1), 90 °C, 18 h, 82−97%; (d) 4′-formylbiphenyl-4-boronic acid, $Pd(PPh_3)_4$, 2 M K_2CO_3, toluene/THF (2:1), 90 °C, 24 h, 80−95%; (e) $PhB(OH)_2$, $Pd(PPh_3)_4$, sat $NaHCO_3$, toluene, 90−100 °C, 12 h, 77%; (f) anhyd $AlCl_3$, C_6H_5COCl, CS_2, reflux, 2.5 h, 81%; (g) excess diphenylmethyl lithium, −20 °C to rt, 3 h, then rt, overnight; (h) PTS, toluene, reflux, overnight, 56−65%.

- the cross arrangement of the dipoles due to the styryl groups is expected to increase luminescence efficiency in the solid state, as has been shown recently by Ma et al.[9]

Herein, we report the synthesis, photophysical, thermal, and electrochemical properties of OPVs **1**−**5**. Their functional behavior is demonstrated by constructing electroluminescent (EL) devices for OPVs **1**−**3**. It is shown that amines with analogous topological features, viz., **BimDPAB**, can be employed as a hole-transporting material (HTM) to yield device electroluminescence efficiency that is ca. 2.5-fold better than with a conventional HTM, viz., *N*, *N*′-bis(naphthalen-1-yl)-*N*,*N*′-bis(phenyl)benzidine (NPB). The three-dimensional bimesitylene-based OPVs **1**−**3** exhibit pure-blue emission close to the National Television Systems Committee (NTSC) standards and exhibit T_g values, EL efficiencies, and brightness that surpass those reported heretofore for simple OPVs lacking amino functionalities.

2. Results

Synthesis of 2- and 4-Fold Phenylenevinylene-Functionalized Bimesitylenes 1−5. The synthesis of OPVs **1**−**5** was accomplished starting from 3,3′-diiodobimesityl **6**[7] and 3,3′,5,5′-tetraiodobimesityl **7**,[7a,10] as shown in Scheme 1. The Suzuki coupling of the diiodobimesityl **6** with 4-formylphenylboronic acid[11] and 4-formylbiphenyl-4′-boronic acid[10] gave the dialdehydes **8** and **9**, respectively. Further treatment of the dialdehydes **8** and **9** with excess of diphenylmethyl lithium followed by acid-catalyzed dehydration

(9) (a) Xie, Z.; Yang, B.; Li, F.; Cheng, G.; Liu, L.; Yang, G.; Xu, H.; Ye, L.; Hanif, M.; Liu, S.; Ma, D.; Ma, Y. *J. Am. Chem. Soc.* **2005**, *127*, 14152. (b) He, F.; Xu, H.; Yang, B.; Duan, Y.; Tian, L.; Huang, K.; Ma, Y.; Liu, S.; Feng, S.; Shen, J. *Adv. Mater.* **2005**, *17*, 2710.

(10) Moorthy, J. N.; Natarajan, R.; Venugopalan, P. *J. Org. Chem.* **2005**, *70*, 8568.

(11) Cousin, D.; Mann, J.; Nieuwenhuyzen, M.; van den Berg, H. *Org. Biomol. Chem.* **2006**, *4*, 54.

TABLE 1. Optical Absorption, Photoluminescence (PL), PL Quantum Yield, Electrochemical Data, and Thermal Properties of 1−5

OPV	λ_{max},[a] nm	band gap,[b] nm (eV)	λ_{max} (PL),[c] soln (solid), nm	Φ_{fl},[d] soln (solid)	HOMO, LUMO,[e] eV	T_d,[f] °C	T_g,[g] °C
1	312	397 (3.12)	439 (447)	0.015 (0.11)	6.03 (6.08), 2.91	438	94
2	326	390 (3.18)	450 (448)	0.01 (0.29)	5.82 (6.05), 2.68	460	123
3	314	366 (3.38)	441 (440)	0.012 (0.06)	6.05 (6.06), 2.68	463	133, 195[h]
4	329	399 (3.11)	444 (473)	0.06 (0.22)	5.82 (6.08), 2.71	495	155, 254[h]
5	315	381 (3.25)	474 (474)	0.004 (0.26)	6.17 (6.08), 2.92	508	152, 251[h]

[a]In cyclohexane solutions (10^{-5} M). [b]Calculated from the absorption onset values. [c]All the emission spectra were recorded for dilute solutions (10^{-6} M) in cyclohexane, λ_{ex} = 367 nm for the solution state and λ_{ex} = 325 nm for the solid state. [d]Quantum yields were determined using anthracene as the standard and N_2 bubbled cyclohexane as the solvent with λ_{ex} = 367 nm. The reported values refer to an average of three independent determinations. The values in parentheses refer to quantum yields for the solid sample/film. [e]HOMO values were calculated from oxidation potentials, while LUMO values were calculated by subtracting the band gap values from the HOMO values. The HOMO values as obtained from UVPES are given in parentheses for comparison. [f]Determined from TGA analyses performed under nitrogen at a heating rate of 10 °C/min. [g]Determined from DSC analyses performed under nitrogen at a heating rate of 10 °C/min. [h]Melting temperature.

afforded the desired disubstituted OPVs **1** and **2**. A similar reaction sequence as above starting from tetraiodobimesityl **7** led to tetrasubstituted diphenylvinyl analogues **3** and **4** in good yields (62−65%). The OPV **5** containing the tetraphenylethylene moiety was prepared starting from **7** in 56% yield via Suzuki coupling, Friedel−Crafts benzoylation, followed by treatment with excess of diphenylmethyl lithium and subsequent dehydration[12] (cf. Experimental Section). The preparation of **Bim-DPAB** has been reported previously.[7b]

Photophysical Properties. In Figure 1, a comparative picture of the UV−vis absorption spectra for **1**−**5** is shown, which shows that all OPVs exhibit λ_{max} within a narrow region (i.e., 312−329 nm). Extension of the arms by changing phenyl to biphenyl (**1**→**2** or **3**→**4**) results in a slight bathochromic shift by ca. 14 nm in the absorption maximum. Introduction of an additional phenyl group into the vinyl double bond does not result in a significant red shift, as is evident from a comparison of the spectra for **3** and **5**. The UV−vis absorption maxima and the band gap energies for all **1**−**5** calculated from their absorption onset potentials are given in Table 1. The solution-state photoluminescence studies for the phenylenevinylenes **1**−**5** show that the emission maxima for **1**−**5** fall in the range of 439−474 nm, with **5** exhibiting a maximum red-shifted emission at 474 nm. Remarkably, all compounds **1**−**5** exhibit blue emission. While the emission for all **1**−**5** was found to be weak in the solution state (Φ_{fl} = 0.004−0.06), strong blue emission was observed in the solid state (Φ_{fl} = 0.06−0.29). A comparison of the emission spectra for **1**−**5** recorded in the solution and solid states (Figure 1) reveals a red shift by ca. 10−30 nm for**1**, **2**, and **4**, while virtually no difference is found in the emission maxima for **3** and **5**. The emission maxima for compounds **1**−**5** along with their photoluminescence quantum yields in both solid and solution states are given in Table 1.

Thermal Properties. The morphological stabilities of OPVs **1**−**5** were gauged by thermogravimetric analysis (TGA) and differential scanning calorimetric (DSC) studies. The TGA analyses show that the thermal decomposition (T_d) values for these compounds are relatively higher (> 400 °C) when compared with their simple DSB analogues (Table 1). The T_d is found to increase with increasing number of phenyl rings attached to the bimesityl core. All of the

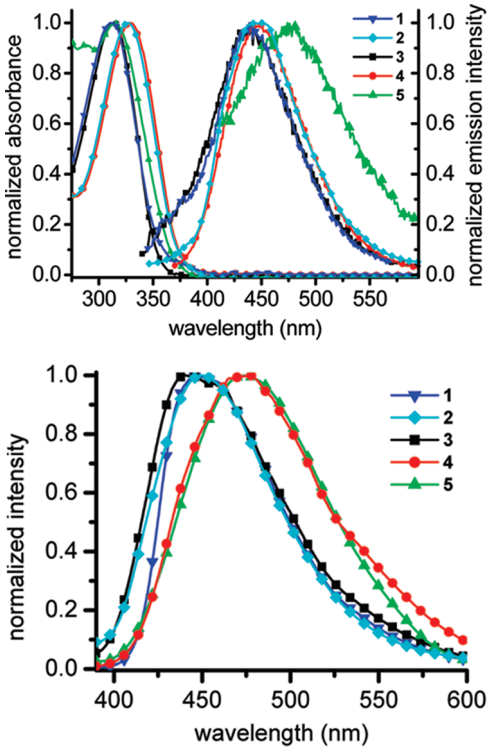

FIGURE 1. UV−vis absorption and PL spectra in cyclohexane (top) and emission spectra in the solid state (bottom) for OPVs **1**−**5**.

phenylenevinylene derivatives of bimesitylene **1**−**5** were found to exhibit stable thermal properties upon several heating and cooling cycles, as revealed by their DSC scans (cf. Supporting Information). The OPV **1** showed T_g at ca. 94 °C without any noticeable presence of crystallization and melting temperatures. In contrast, it is noteworthy that the commercial blue-emitter, viz., 4,4′-diphenylvinylbiphenyl, shows glass transition at 64 °C and crystallizes at 106 °C.[5a,6] The 4-fold-functionalized analogue **3** exhibited glass transition at 133 °C followed by an endothermic transition at 195 °C. The phenyl extended disubstituted bimesityl derivative **2** displayed a stable glass transition temperature at ca. 123 °C without melting up to 400 °C. The analogous 4-fold derivative **4** showed glass transition at ca. 155 °C. The tetraphenylethylene-functionalized bimesityl **5** exhibited T_g at 152 °C but revealed a broad endothermic melting transition at around 251 °C. Clearly, the three-dimensional D_{2d}-symmetric bimesitylene

(12) Banerjee, M.; Emond, S. J.; Lindeman, S. V.; Rathore, R. *J. Org. Chem.* **2007**, *72*, 8054.

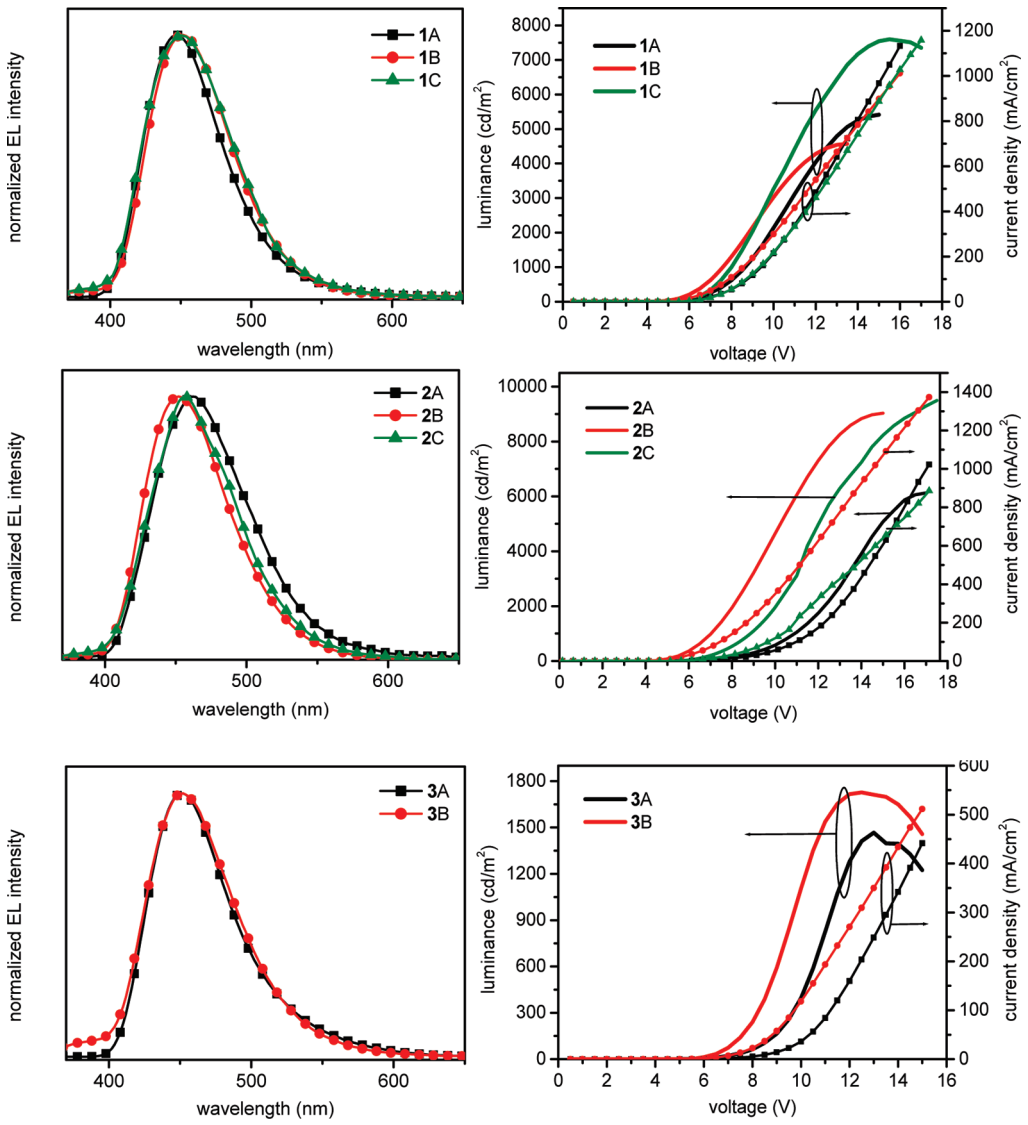

FIGURE 2. EL spectrum (left) and the $I-V-L$ curves (right) of the devices of **1**−**3**. The device configurations are (**1**A) ITO/NPB (400 Å)/**1** (100 Å)/BCP (100 Å)/Alq_3 (300 Å)/LiF (10 Å)/Al (1500 Å); (**1**B) ITO/NPB (400 Å)/**1** (100 Å)/TPBI (400 Å)/LiF (10 Å)/Al (1500 Å); (**1**C) ITO/NPB (300 Å)/CBP (200 Å)/**1** (100 Å)/TPBI (400 Å)/LiF (10 Å)/Al (1500 Å); (**2**A) ITO/NPB (400 Å)/**2** (100 Å)/BCP (100 Å)/ Alq_3 (300 Å)/LiF (10 Å)/Al (1500 Å); (**2**B) ITO/NPB (400 Å)/**2** (100 Å)/TPBI (400 Å)/LiF (10 Å)/Al (1500 Å); (**2**C) ITO/NPB (300 Å)/CBP (200 Å)/**2** (100 Å)/TPBI (400 Å)/LiF (10 Å)/Al (1500 Å); (**3**A) ITO/NPB (400 Å)/**3** (100 Å)/BCP (100 Å)/Alq_3 (300 Å)/LiF (10 Å)/Al (1500 Å); (**3**B) ITO/NPB (400 Å)/**3** (100 Å)/TPBI (400 Å)/LiF (10 Å)/Al (1500 Å).

core discourages close packing of molecules and hence crystallization to impart amorphous glassy nature.

Electrochemical Properties. The cyclic voltammetric (CV) measurements were carried out for **1**−**5** in order to determine the HOMO and LUMO energy levels (cf. Supporting Information). The HOMO values were calculated from the oxidation potentials (E_{ox}) and were compared with the ionization potentials determined from the UV photoelectron spectroscopic measurements. The LUMOs were calculated from their respective onset potentials (band gap energy) obtained from the tail-end of the absorption spectra and HOMO values. The di- and tetra-substituted bimesitylene derivatives exhibited similar HOMO and LUMO values (Table 1), which attests to the absence of communication between the chromophores linked at the *meta* sites. The HOMO values of the OPVs were found to be as low as ca. 6.0 eV with optical band gap energy higher than 3.0 eV.

Electroluminescence Properties. The functional behavior of OPVs **1**−**5** was investigated by fabricating devices for **1**−**3**, as representative cases, to capture electroluminescence. The 2-fold-functionalized (**1** and **2**) and 4-fold-functionalized bimesitylene (**3**) were conveniently vacuum sublimed to construct multilayer nondoped devices, which comprised four types: (A) ITO/NPB (400 Å)/**1**−**3** (100 Å)/BCP (100 Å)/ Alq_3 (300 Å)/LiF (10 Å)/Al (1500 Å), (B) ITO/NPB (400 Å)/**1**−**3** (100 Å)/TPBI (400 Å)/LiF (10 Å)/Al (1500 Å), (C) ITO/NPB (300 Å)/CBP (200 Å)/**1**−**2** (100 Å)/TPBI (400 Å)/ LiF (10 Å)/Al (1500 Å), and (D) ITO/**Bim-DPAB** (400 Å)/**2** (100 Å)/TPBI (400 Å)/LiF (10 Å)/Al (1500 Å), where ITO (indium tin oxide) was the anode, NPB or **Bim-DPAB** (3,3′-bis(4-diphenylaminobiphenyl-4′-yl)bimesityl served as the hole-transporting layer, CBP (4,4′-bis(carbazol-9-yl)biphenyl) served as the electron-blocking layer, **1**/**2**/**3** as the emitting layer, BCP (bathocuprine) as a hole-blocking material, TPBI

TABLE 2. Electroluminescence Data for 1−3

device[a]	V_{on}[b]	η_{ex}[c]	η_p[d]	η_l[e]	λ_{max}^{EL}	L_{max}[f]	CIE[g] x, y
1A	4.5	1.52	0.55	1.22	448	5415	0.15, 0.09
1B	4.5	1.51	0.66	1.29	452	4575	0.14, 0.08
1C	5.0	2.21	0.93	1.90	450	7599	0.15, 0.10
2A	4.5	1.07	0.49	1.38	462	6129	0.10, 0.16
2B	4.5	1.95	0.95	1.80	452	9031	0.14, 0.11
2C	5.0	2.11	1.10	2.24	456	9500	0.15, 0.13
2D	4.5	4.70	2.02	5.40	460	15361	0.15, 0.17
3A	5.0	1.06	0.39	1.15	452	1466	0.16, 0.13
3B	5.5	1.08	0.43	1.07	452	1727	0.15, 0.12

[a]The four types of devices are (A) ITO/NPB (400 Å)/**1**−**3** (100 Å)/BCP (100 Å)/Alq_3 (300 Å)/LiF (10 Å)/Al (1500 Å), (B) ITO/NPB (400 Å)/**1**−**3** (100 Å)/TPBI (400 Å)/LiF (10 Å)/Al (1500 Å), (C) ITO/NPB (300 Å)/CBP (200 Å)/**1**−**2** (100 Å)/TPBI (400 Å)/LiF (10 Å)/Al (1500 Å), (D) ITO/**Bim-DPAB** (400 Å)/**2** (100 Å)/TPBI (400 Å)/LiF (10 Å)/Al (1500 Å). [b]Turn-on voltage. [c]External quantum efficiency (%) at 20 mA/cm^2. [d]Power efficiency (lm/W) at 20 mA/cm^2. [e]Luminance efficiency (cd/A) at 20 mA/cm^2. [f]Maximum luminance achieved (cd/m^2). [g]1931 CIE chromaticity coordinates.

(2,2′,2″-(1,3,5-benzenetriyl)-tris(1-phenyl-1*H*-benzimidazole)/Alq_3 (tris(8-hydroxyquinolinato)aluminum) as an electron-transporting layer, and LiF/Al as the composite cathode. The EL spectra and $I-V-L$ characteristics of the devices **1**A-C, **2**A-C, and **3**A-B are shown in Figure 2. The performance characteristics for these devices are presented in Table 2. Clearly, the nondoped devices constructed for OPVs **1**−**3** revealed excellent pure-blue emission according to the NTSC standards with CIE coordinates (Commission Internationale de l'Eclairge) equal to or nearest to $x = 0.14$, $y = 0.08$; the chromaticity diagram for the blue light emission from the EL devices of **1**−**3** (types A and B) is displayed in Figure 3. The device turn-on voltages were as low as 4.5−5.5 V. The external quantum efficiencies of these nondoped devices of standard configurations were found to vary from 1.1 to 1.5% for BCP/Alq_3-based devices and 1.1−2.0% for TPBI-based devices at a current density of 20 mA/cm^2. The color purity as well as the performance of TPBI-based devices is, in general, better as compared to that of BCP/Alq_3-based devices.[13] Hence, further modifications were attempted on the device structure of the TPBI-based devices (type B) in order to improve the device efficiencies for **1** and **2**. Insertion of additional electron-blocking CBP (4,4′-bis-(carbazol-9-yl)biphenyl) layer between the emitting layer and the hole-transporting layer in device type B for OPVs **1** and **2** led to considerable increase in the device efficiency (up to 2.22% for **1**) as well as in the luminance efficiency (up to 2.28 cd/A for **2**) with a marginal change in color purity (cf. Supporting Information). Remarkably, replacement of the hole-transporting layer involving NPB with **Bim-DPAB**, an HTM with structural characteristics similar to those of OPVs **1**−**5**, in the case of the device **2**B for OPV **2**, that is, ITO/**Bim-DPAB** (400 Å)/**2** (100 Å)/TPBI (400 Å)/LiF (10 Å)/Al (1500 Å), resulted in a dramatic improvement in the device efficiencies; the external quantum efficiency of the above device reached as high as 4.70% (20 mA/cm^2), which is higher than those reported for nondoped pure-blue emitters based on OPVs reported so far.[9,14]

3. Discussion

Enormous commercial success with π-conjugated polymers/oligomers in OLEDs has spurred a great deal of interest in the development of blue-light-emitting π-conjugated molecules that display desirable optoelectronic properties. There has been an emphasis of interest in blue-light-emitting materials in particular, as they can be used to generate white light emission.[14a,b,15] Besides, it has been shown that the purity of blue emission is inversely related to the consumption of power for full-color displays. Thus, the blue-light-emitting molecular materials based on OPVs **1**−**5**, which are of intermediate dimension, offer tremendous advantage over other materials from the point of view of ease of processability. The linkage of additional phenyl rings, as in **4** and **5**, leads to increase in decomposition (T_d) as well as the glass transition temperatures (T_g) considerably (Table 1). The attachment of additional phenyl rings evidently contributes to some steric congestion and bulkiness of the molecules, leading to better and stable morphological behavior, as reflected by the device characteristics; highly stable glassy nature is what is most desired of a material to be employed in OLEDs. The extension of π-conjugation by way of attachment of an additional phenyl ring does result in a marginal bathochromic shift of the λ_{max} (UV−vis or PL) such that the optical properties may be appropriately modulated. In the case of 4-fold derivatives **3**−**5**, the π-conjugation is limited to the attached unit, and there exists only a weak *meta*-conjugation or communication between the units linked to the central mesitylene ring. The presence of the additional phenyl groups on the periphery of OPVs **3**−**5** may force a nonplanar geometry of the π-system (C=C) due to sterically congested environment around the double bond.[16] The effect of *meta*-conjugation and the effect of attachment of additional phenyl ring on fluorescence can be readily discerned when moving from **1** to **3** to **5**.[16b,17] It is well-known that the emission of multisubstituted olefins depends not only on the nature of the aryl groups but also on the position of their attachment on to the olefins.[16] A marginal red shift observed in the emission of solid films, in general, may be attributed to the difference in the media. The solid-state quantum efficiencies of all the OPVs are greater than those observed in the solution state. The poor solution-state quantum efficiencies

(13) For example, see: (a) Tao, Y. T.; Balasubramaniam, E.; Daniel, A.; Wilsa, A.; Tomasik, P. *J. Mater. Chem.* **2001**, *11*, 768. (b) Thomas, K. R. J.; Velusamy, M.; Lin, J. T.; Chuen, C. H.; Tao, Y. T. *J. Mater. Chem.* **2005**, *15*, 4453.

(14) (a) van Hutten, P. F.; Wildeman, J.; Meetsma, A.; Hadziioannoou, G. *J. Am. Chem. Soc.* **1999**, *121*, 5910. (b) Cheon, K. O.; Shinar, J. *Appl. Phys. Lett.* **2002**, *81*, 1738. (c) Xie, W.; Hou, J.; Liu, S. Y. *Semicond. Sci. Technol.* **2003**, *18*, 42.

(15) (a) Kido, J.; Kimura, M.; Nagai, K. *Science* **1995**, *267*, 1332. (b) Strukelj, M.; Jordan, R. H.; Dodabalapur, A. *J. Am. Chem. Soc.* **1996**, *118*, 1213. (c) D'Andrade, B. W.; Thompson, M. E.; Forrest, S. R. *Adv. Mater.* **2000**, *12*, 130. (d) D'Andrade, B. W.; Brooks, J.; Adamovich, V.; Thompson, M. E.; Forrest, S. R. *Adv. Mater.* **2002**, *14*, 1032. (e) Zhang, X. H.; Liu, M. W.; Wong, O. Y.; Lee, C. S.; Kwong, H. L.; Lee, S. T.; Wu, S. K. *Chem. Phys. Lett.* **2003**, *369*, 478. (f) Chuen, C. H.; Tao, Y. T.; Wu, F. I.; Shu, C. F. *Appl. Phys. Lett.* **2004**, *85*, 4609. (g) Mita, Y.; Kobayashi, T.; Miyamoto, Y.; Ishii, O.; Sawanobori, N. *Phys. Status Solidi B* **2004**, *241*, 2672. (h) D'Andrade, B. W.; Forrest, S. R. *Adv. Mater.* **2004**, *16*, 1585. (i) Mazzeo, M.; Vitale, V.; Sala, F. D.; Anni, M.; Barbarella, G.; Favaretto, L.; Sotgiu, G.; Cingolani, R.; Gigli, G. *Adv. Mater.* **2005**, *17*, 34. (j) Cheng, G.; Xie, Z.; Zhao, Y.; Zhang, Y.; Xia, H.; Ma, Y.; Liu, S. *Thin Solid Films* **2005**, *484*, 54. (k) Yang, Y.; Lowry, M.; Schowalter, C. M.; Fakayode, S. O.; Escobedo, J. O.; Xu, X.; Zhang, H.; Jensen, T. J.; Fronczek, F. R.; Warner, I. M.; Strongin, R. M. *J. Am. Chem. Soc.* **2006**, *128*, 14081 and references cited therein.

(16) (a) Itami, K.; Tonogaki, K.; Ohashi, Y.; Yoshida, J. *Org. Lett.* **2004**, *6*, 4093. (b) Itami, K.; Ohashi, Y.; Yoshida, J. *J. Org. Chem.* **2005**, *70*, 2778. (c) Itami, K.; Yoshida, J. *Bull. Chem. Soc. Jpn.* **2006**, *79*, 811.

(17) Banerjee, M.; Emond, S. J.; Lindeman, S. V.; Rathore, R. *J. Org. Chem.* **2007**, *72*, 8054.

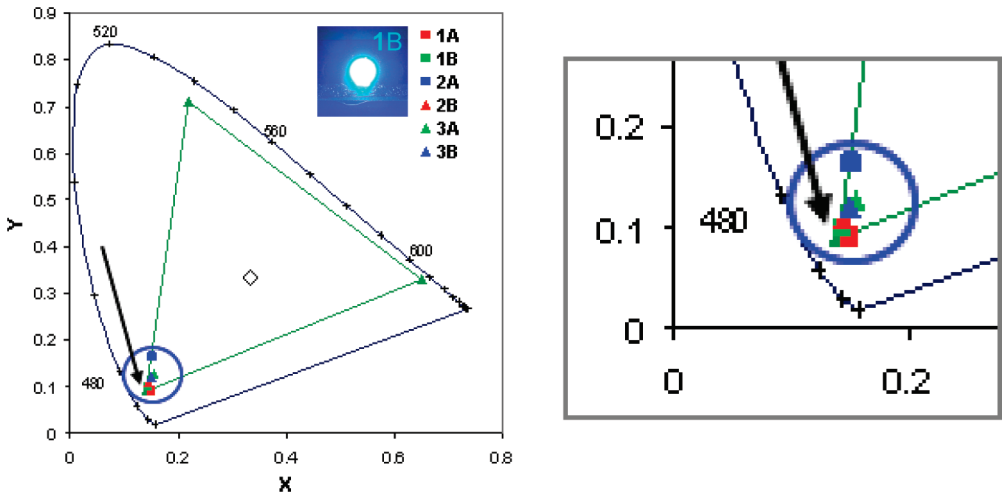

FIGURE 3. CIE chromaticity diagram (left) for the nondoped devices (A and B) constructed from OPVs **1**−**3**. The circle indicates the pure-blue emission region according to the NTSC standards. The enlarged view of this region is shown in the right. The inset photograph shows the blue electroluminescence captured from device **1B**.

in all of these cases are undoubtedly due to efficient isomerization, which is characteristic of stilbenes.[18] The respectable solid-state quantum efficiencies of OPVs **1**−**5** and the absence of long wavelength emission band in their PL of solid/films suggests that the molecular topology prevents efficient molecular packing and hence aggregation, thereby reducing the intermolecular interactions and hence fluorescence quenching, leading to significantly improved solid-state luminescence properties (ca. 10−60-fold). Very recently, several examples such as styrylbenzene derivatives,[19] arylethynylenes,[20] siloles,[21] polymers,[22] and others[23] have been shown to display better emission in the solid state than in the solution state. Though the origin of such enhanced emission in the solid state is still not unambiguously clear, it is presumed that the sole phenomenon of change in emission is mostly linked to the inter- and intramolecular effects; while the twisted (solution state) and the planar (solid state) conformations affect (suppress and promote the radiation process, respectively) the fluorescence change intramolecularly,[19a,g] the type of aggregation (H- or J-aggregation) influences the emission efficiency. H-aggregates induce nonradiative deactivation process, while J-aggregates trigger the radiative process intermolecularly.[24] The nonplanar sterically congested environment of the vinylene/ethylene double bond in addition to the crossed arrangement of the chromophores in the D_{2d}-symmetric 4-fold-functionalized OPVs **3**−**5** presumably contributes to the restricted molecular motions that promote radiative fluorescence enhancement in the solid state.[16b,c] As mentioned earlier, it has been predicted by Bredas et al.[25] from theoretical analysis that the nonplanar perpendicular arrangement of transition dipoles of the chromophores avoids fluorescence quenching and promotes the solid-state luminance efficiency. Also, Ma et al. have recently demonstrated this feature in dimeric and trimeric DSBs.[9b,26] Indeed, such materials appear to be relevant for application in solid-state lasers.[9a,27]

Remarkably, all OPVs exhibit a uniform oxidation behavior in the CV in that the di- and the tetra-substituted derivatives show similar oxidation potentials. These blue-emitting OPVs with reasonable band gap energies (ca. 3.11−3.38 eV) may in principle be used in the generation of full-color displays. The ready sublimation of OPVs **1**−**3** permitted facile fabrication of multilayer devices to capture the pure-blue electroluminescence (λ_{max} = 448−462 nm). Although the OPVs **1**−**5** possess large band gap energies, their low turn-on voltages from 4.5 to 5.5 V reveal that the charge injection in these materials is really not difficult. It is noteworthy that the blue-emitting materials suffer from charge injection in general. Of the two types of nondoped devices (A and B) fabricated, the device B was found to perform better than A. The device from OPV **2** [**2**B: ITO/NPB (400 Å)/**2** (100 Å)/TPBI (400 Å)/LiF (10 Å)/Al (1500 Å)] shows best performance with a bright blue luminance of 9031 cd/m^2 and a luminance efficiency of 1.8 cd/A at 20 mA/cm^2. The external quantum efficiency and the CIE coordinates of the above device are 2.0% and x = 0.14 and y = 0.11, respectively

(18) Waldeck, D. H. *Chem. Rev.* **1991**, *91*, 415.
(19) (a) An, B. K.; Kwon, S. K.; Jung, S. D.; Park, S. Y. *J. Am. Chem. Soc.* **2002**, *124*, 14410. (b) Lim, S. J.; An, B. K.; Jung, S. D.; Chung, M. A.; Park, S. Y. *Angew. Chem., Int. Ed.* **2004**, *43*, 6346. (c) Yeh, H. C.; Yeh, S. J.; Chen, C. T. *Chem. Commun.* **2003**, 2632. (d) Chen, J.; Xu, B.; Ouyang, X.; Tang, B. Z.; Cao, Y. *J. Phys. Chem. A* **2004**, *108*, 7522. (e) Bhongale, C. J.; Chang, C. W.; Lee, C. S.; Diau, W. G.; Hsu, C. S. *J. Phys. Chem. B* **2005**, *109*, 7522. (f) Xie, Z.; Yang, B.; Cheng, G.; Liu, L.; He, F.; Shen, F.; Ma, Y.; Liu, S. *Chem. Mater.* **2005**, *17*, 1287. (g) Xie, Z.; Yang, B.; Xie, W.; Liu, L.; Shen, F.; Wang, H.; Yang, X.; Wang, Z.; Li, Y.; Hanif, M.; Yang, G.; Ye, L.; Ma, Y. *J. Phys. Chem. B* **2006**, *110*, 20993.
(20) Levitus, M.; Schmieder, K.; Ricks, H.; Shimizu, K. D.; Bunz, U. H. F.; Garcia-Garibay, M. A. *J. Am. Chem. Soc.* **2001**, *123*, 4259.
(21) Fan, X.; Sun, J.; Wang, F.; Chu, Z.; Wang, P.; Dong, Y.; Hu, R.; Tang, B. Z.; Zou, D. *Chem. Commun.* **2008**, 2989 and references cited therein.
(22) (a) Deans, R.; Kim, J.; Machacek, M. R.; Swager, T. M. *J. Am. Chem. Soc.* **2000**, *122*, 8565. (b) Belton, C.; O'Brien, D. F.; Blau, W. J.; Cadby, A. J.; Lane, P. A.; Bradley, D. D. C.; Byrne, H. J.; Stockman, R.; Hörhold, H. H. *Appl. Phys. Lett.* **2001**, *78*, 1059.
(23) Wang, Z.; Shao, H.; Ye, J.; Tang, L.; Lu, P. *J. Phys. Chem. B* **2005**, *109*, 19627.
(24) Rösch, U.; Yao, S.; Wortmann, R.; Würthner, F. *Angew. Chem., Int. Ed.* **2006**, *45*, 7026 and references therein.
(25) Cornil, J.; Beljonne, D.; Calbert, J. P.; Brédas, J. L. *Adv. Mater.* **2001**, *13*, 1053.
(26) (a) He, F.; Cheng, G.; Zhang, H. Q.; Zheng, Y.; Xie, Z. Q.; Yang, B.; Ma, Y.; Liu, S. Y.; Chen, J. C. *Chem. Commun.* **2003**, 2206. For cruciform DPVBi, see: (b) Liu, S.; He., F.; Wang, H.; Xu, H.; Wang, C.; Li, F.; Ma, Y. *J. Mater. Chem.* **2008**, *18*, 4802.
(27) (a) Johansson, N.; Salbeck, J.; Bauer, J.; Weissortel, F.; Broms, P.; Anderson, A.; Salaneck, W. R. *Adv. Mater.* **1998**, *10*, 1136. (b) Spehr, T.; Pudzich, R.; Fuhrmann, T.; Salbeck, J. *Org. Electron.* **2003**, *4*, 61.

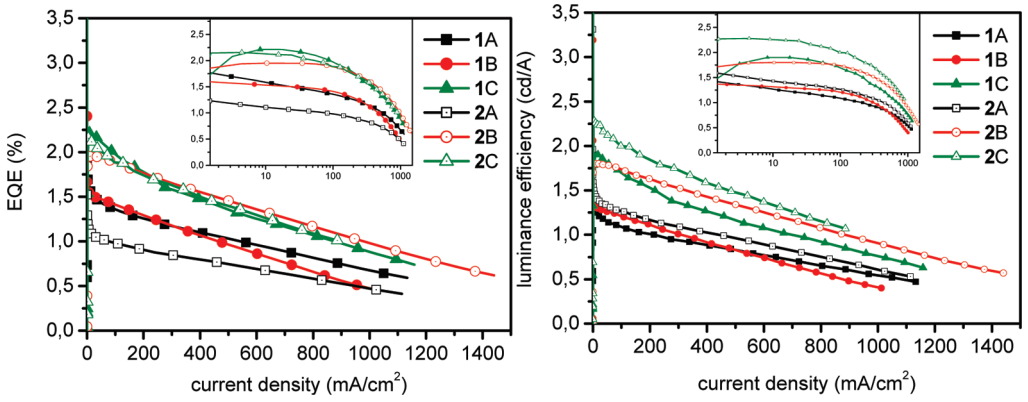

FIGURE 4. External and luminance quantum efficiencies of the nondoped devices **1**A−C and **2**A−C.

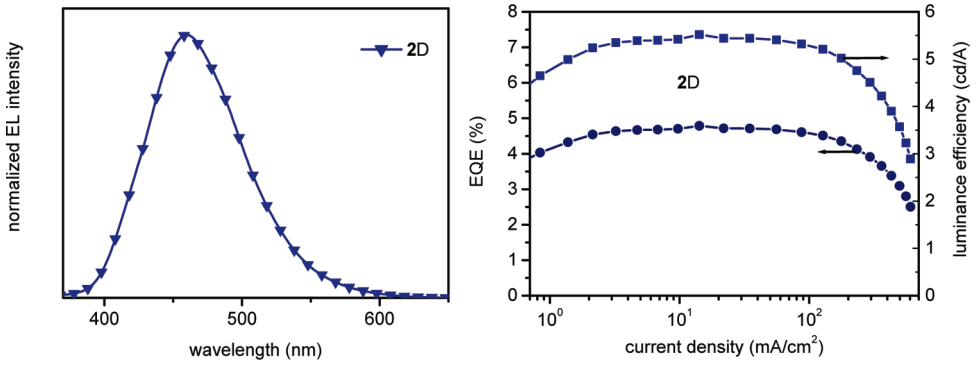

FIGURE 5. EL spectrum and external and luminance quantum efficiencies of the device **2**D. The device configuration of **2**D was ITO/**Bim-DPAB** (400 Å)/**2** (100 Å)/TPBI (400 Å)/LiF (10 Å)/Al (1500 Å).

(Figure 4 and Table 2). The best device of **1** was achieved by insertion of the additional CBP layer (HOMO = 5.7 eV and LUMO = 2.0 eV)[28] between NPB and the emitting material **1** [**1**C: ITO/NPB (300 Å)/CBP (200 A)/**1** (100 Å)/TPBI (300 Å)/LiF (10 Å)/Al (1500 Å)]. This promotes the efficient hole−electron recombination to occur in the emitting layer (**1**) by reducing the energy barrier for hole injection between NPB (HOMO = 5.4 eV)[29] and **1**, and by blocking the electrons from entering into NPB very readily. Thus, the modified device showed a maximum luminance of 7599 cd/m^2 with an increased external quantum efficiency of 2.22% and a luminance efficiency of 1.90 cd/A at 20 mA/cm^2 (Figure 4). At a brightness of 800 cd/m^2, devices **1**C and **2**C exhibited external quantum efficiencies of 2.14 and 2.04% at current density = 41.75 mA/cm^2 (7.71 V) and a luminance efficiencies of 1.84 and 2.18 cd/A at current density = 35.06 mA/cm^2 (8.49 V). Such high external quantum and luminance efficiencies based on a simple device structure for OPVs **1** and **2** are indeed remarkable. To our excitement, the device **2**D with a HTL based on structurally analogous bimesityl-based amine, viz., **Bim-DPAB**, led to excellent performance characteristics when compared to all other devices that were fabricated. The external quantum efficiency for the device **2**D with **Bim-DPAB** increased dramatically from 1.97% (**2**B) to 4.70% (2.5-fold) with a corresponding enhancement in the luminance efficiency from 1.80 cd/A (**2**B) to 5.40 cd/A at current density = 20 mA/cm^2; the maximum external and luminance efficiencies were 4.79 and 5.52%, respectively, at a current density of 14.22 mA/cm^2 (9.0 V) with the power efficiency being 2.44 lm/W at 6 V (0.84 mA/cm^2). The EL spectrum and the performance efficiency of the device **2**D are given in Figure 5. Given that the HOMO values of NPB[29] and **Bim-DPAB** (5.54 eV) are closer, the origin of the excellent performance of device **2**D should be attributed to the morphological compatibility of the hole-transporting and emitting layers, both of which are uniquely based on the bimesitylene scaffold.

It is well-known that amorphous layers that are pinhole-free facilitate charge mobilities and their recombination efficiently. Thus, the fantastic amorphous property imparted by the bimesitylene core with orthogonal planes in bringing about morphological compatibility of the two layers is compellingly evident from the device characteristics. There are only scant reports of layer compatibility studies so far in OLEDs with appropriately designed materials; for example, the EL device constructed using spiro-based HTL (spiro-TAD) and ETL (spiro-PBD) showed good performance.[30]

(28) (a) Chen, C.-H.; Wu, F.-I.; Shu, C.-F.; Chien, C.-H.; Tao, Y.-T. *J. Mater. Chem.* **2004**, *14*, 1585. (b) Chow, T. J.; Lin, R.; Ko, C.-W.; Tao, Y.-T. *J. Mater. Chem.* **2002**, *1*, 42.

(29) (a) Tong, Q.-X.; Lai, S.-L.; Chan, M.-Y.; Lai, K.-H.; Tang, J.-X.; Kwong, H.-L.; Lee, C.-S.; Lee, S.-T. *Chem. Mater.* **2007**, *19*, 5851. (b) Wu, Z.; Yang, H.; Duan, Y.; Xie, W.; Liu, S.; Zhao, Y. *Semicond. Sci. Technol.* **2003**, *18*, 49.

(30) Salbeck, J.; Yu, N.; Bauer, J.; Weissortel, F.; Bestgen, H. *Synth. Met.* **1997**, *91*, 209.

The characteristics of the nondoped devices of OPVs **1**−**3** described herein are comparatively better than those for the commonly used blue dopant such as DPVBi,[14b,c] and oligomeric PPVs *do not* contain amino substituents.[5a,9,26,31] It should be mentioned that even the 4-fold-functionalized bimesitylenes such as **3** can be comfortably sublimed without any residual traces.

4. Conclusions

The 2-fold- and 4-fold-functionalized phenylenevinylenes **1**−**5** based on three-dimensional D_{2d}-symmetric bimesitylene scaffold constitute a new family OPVs, whose advantages include unique pattern of substitution, ease of synthesis, and molecular topology that prevents ready crystallization leading to amorphous nature. The bimesityl core is simply a bystander permitting the optical properties of the attached chromophores to be reproduced, while assuring enhancement of fluorescence emission efficiency in the solid state via crossed arrangement of chromophores, amorphous nature, and high T_g values. The increase in the conjugation of the chromophores leads to corresponding variation in the absorption and emission properties, whereby the modulation of photophysical properties is readily achieved. The functional behavior of this new class of amorphous materials is demonstrated from electroluminescence studies, which reveal emission properties that surpass the ones reported for nondoped blue-light emitters based on the same category. It is shown that both hole-transporting and emitting materials (i.e., **Bim-DPAB** and OPV **2**) based on analogous structural characteristics show remarkable layer compatibility to permit electroluminescence with extraordinary efficiencies. Clearly, the strategy based on the bimesitylene scaffold opens way for a myriad of amorphous pure-blue emitting materials with desirable thermal stability.

5. Experimental Section

General Aspects: All Pd(0)-mediated cross-coupling reactions were performed under a nitrogen gas atmosphere in oven-dried pressure tubes. ^{1}H and ^{13}C NMR spectra were recorded on a 400/500 MHz spectrometer in $CDCl_3$ as a solvent. Chemical shifts are reported in δ scale downfield from tetramethylsilane. The FAB-mass spectra were recorded on a mass system using argon/xenon as the FAB gas in a linear mode with *m*-nitrobenzyl alcohol as the matrix. The TGA and DSC measurements were carried out at 10 °C/min under a nitrogen gas atmosphere. The photoluminescence spectra in the solution state were recorded using spectral grade solvents, and those of the thin solid films were measured by front-face excitation and detection. The ionization potentials were calculated by photoelectron spectroscopy with UV intensity of 5−30 nW. The Commission Internationale de l'Eclairage (CIE) coordinates of the devices were measured by a spectroscan spectrometer.

Materials: Dry tetrahydrofuran (THF) and toluene were freshly distilled over sodium prior to use. All of the reactions were monitored by analytical thin layer chromatography (TLC) using commercial aluminum sheets precoated with silica gel. Chromatography was conducted on silica gel of mesh size 60−120. All of the commercial chemicals were used as received. The starting materials, viz., bimesityl,[7] diiodobimesityl,[7] tetraiodobimesityl,[7] 3,3′,5,5′-tetrakis(4-formylphenyl)bimesityl,[10] and 3,3′,5,5′-tetrakis[4(4′-formyl)biphenyl]bimesityl,[10] were synthesized according to the earlier reported procedures established in our laboratories. The detailed synthetic procedures for preparing **1**−**5** are given below (cf. Scheme 1).

Preparation of 3,3′-Diiodobimesityl (6):[7]**.** In a two-necked round-bottom flask, bimesityl (0.40 g, 1.68 mmol) was dissolved in CH_3CN (8 mL). To this was added NIS (0.83 g, 3.69 mmol) followed by TFA (0.08 mL) under vigorously stirring cold conditions (5 °C). The reaction mixture was allowed to stir at room temperature for 8 h. Subsequently, the reaction mixture was concentrated, and the organic matter was extracted with $CHCl_3$. The combined extract was washed with $NaHCO_3$ solution followed by brine, dried over anhyd Na_2SO_4, filtered, and evaporated to dryness. A careful silica gel column chromatography using $CHCl_3$ and petroleum ether mixture (1:9) afforded the colorless compound diiodobimesityl **6** in 83% yield (0.68 g): IR (KBr) cm^{-1} 2970, 2947, 2915, 1449, 1375; ^{1}H NMR ($CDCl_3$, 400 MHz) δ 1.78 (s, 6H), 2.07 (s, 6H), 2.48 (s, 6H), 7.03 (s, 2H); ^{13}C NMR ($CDCl_3$, 100 MHz) δ 19.6, 26.7, 29.9, 106.2, 129.0, 135.2, 138.3, 138.8, 140.7.

Preparation of 3,3′-Bis(4-formylphenyl)bimesityl (8): A 120 mL pressure tube, removed hot from oven, was cooled under N_2 atmosphere and charged with diiodobimesityl **6** (1.80 g, 3.67 mmol), 4-formylphenylboronic acid (1.65 g, 11.02 mmol), Pd(PPh_3)$_4$ (0.254 g, 0.22 mmol), toluene (20 mL), THF (10 mL), and 2 M K_2CO_3 solution (10 mL). The mixture was bubbled with a N_2 gas for 20 min, the pressure tube was capped tightly, and the reaction mixture was heated at 90 °C. The yellow turbid solution became clear in 2 h. The heating was continued for a further 16 h, after which time the color of the reaction mixture turned dark brown. At this stage, the reaction mixture was cooled and extracted with ethyl acetate. The combined extracts were washed with water and brine, dried over anhyd Na_2SO_4, filtered, and concentrated. The pure product **8** was isolated as a pale yellow solid (1.6 g, 97%) by column chromatography with silica gel using ethyl acetate and petroleum ether mixture (5:95) as an eluent: mp 242−244 °C; IR (KBr) cm^{-1} 3003, 2918, 2820, 1706, 1603; ^{1}H NMR ($CDCl_3$, 500 MHz) δ 1.59 (s, 6H), 1.94 (s, 6H), 2.01 (s, 6H), 7.06 (s, 2H), 7.34 (dd, J_1 = 16.0 Hz, J_2 = 7.75 Hz, 4H), 7.93 (t, J = 8.2 Hz, 4H), 10.05 (s, 2H); ^{13}C NMR ($CDCl_3$, 125 MHz) δ 17.8, 19.9, 20.7, 129.2, 129.90, 129.92, 130.3, 132.8, 133.7, 134.9, 135.1, 138.0, 138.7, 148.7, 192.0; FAB-MS $(M + H)^+$ 447.

Preparation of 3,3′-Bis(4(4′-formyl)biphenyl)bimesityl (9): This compound was synthesized using 4′-formylbiphenyl-4-boronic acid following the procedure used for the preparation of 3,3′-bis(4-formylphenyl)bimesityl, **8**: yield 95%; mp 196−198 °C; IR (KBr) cm^{-1} 3024, 2917, 2855, 1695, 1601; ^{1}H NMR ($CDCl_3$, 500 MHz) δ 1.69 (s, 6H), 1.98 (s, 6H), 2.08 (s, 6H), 7.08 (s, 2H), 7.29 (dd, J_1 = 14.4 Hz, J_2 = 8.0 Hz, 4H), 7.70 (t, J = 8.94 Hz, 4H), 7.82 (d, J = 8.2 Hz, 4H), 7.96 (d, J = 8.2 Hz, 4H), 10.05 (s, 2H); ^{13}C NMR ($CDCl_3$, 125 MHz) δ 17.9, 19.9, 20.9, 127.3, 127.5, 128.9, 130.2, 130.3, 133.3, 134.1, 134.6, 135.1, 137.6, 138.1, 139.2, 142.3, 146.9, 191.9; FAB-MS $(M + H)^+$ 599.

Preparation of 3,3′,5,5′-Tetrakis(4-formylphenyl)bimesityl:[10]**.** This compound was synthesized using 4-formylphenylboronic acid following the procedure used for the preparation of 3,3′-bis(4-formylphenyl)bimesityl, **8**: yield 82%; mp 280−282 °C (dec); IR (KBr) cm^{-1} 3045, 1699, 1603; ^{1}H NMR (400 MHz, $CDCl_3$) δ 1.67 (s, 6H), 1.68 (s, 12 H), 7.39 (d, 8H, J = 8.04 Hz), 7.96 (d, 8H, J = 8.04 Hz), 10.07 (s, 4H); ^{13}C NMR (100 MHz, $CDCl_3$) δ 18.3, 19.2, 130.0, 130.2, 131.4, 132.6, 135.0, 138.5, 139.3, 148.7, 192.0; FAB-MS (M + 1) 655.

(31) (a) Ostrowski, J. C.; Hudack, R. A. Jr.; Robinson, M. R.; Wang, S.; Bazan, G. C. *Chem.—Eur. J.* **2001**, *7*, 4500. (b) Robinson, M. R.; Wang, S.; Heeger, A. J.; Bazan, G. C. *Adv. Funct. Mater.* **2001**, *11*, 413. (c) Cheng, G.; He, F.; Zhao, Y.; Duan, Y.; Zhang, H.; Yang, B.; Ma, Y.; Liu, S. *Semicond. Sci. Technol.* **2004**, *19*, 78. (d) He, F.; Xia, H.; Tang, S.; Duan, Y.; Zeng, M.; Liu, L.; Li, M.; Zhang, H.; Yang, B.; Ma, Y.; Liu, S.; Shen, J. *J. Mater. Chem.* **2004**, *14*, 2735. (e) Niazimbetova, Z. I.; Christian, H. Y.; Bhandari, Y. J.; Beyer, F. L.; Galvin, M. E. *J. Phys. Chem. B* **2004**, *108*, 8673. (f) Rathnayake, H. P.; Cirpan, A.; Lahti, P. M.; Karasz, F. E. *Chem. Mater.* **2006**, *18*, 560.

Preparation of 3,3′,5,5′-Tetrakis(4(4′-formyl)biphenyl)bimesityl:[10]**.** This compound was synthesized using 4′-formylbiphenyl-4-boronic acid following the procedure used for the preparation of 3,3′-bis(4-formylphenyl)bimesityl, **8**: yield 80%; mp 160−162 °C, IR (KBr) cm^{-1} 3028, 2923, 1697; ^1H NMR ($CDCl_3$, 400 MHz) δ 1.78 (s, 12 H), 1.81 (s, 6H), 7.36 (d, 8H, J = 8.32 Hz), 7.74 (d, 8H, J = 8.32 Hz), 7.85 (d, 8H, J = 8.32 Hz), 7.98 (d, 8H, J = 8.32 Hz), 10.07 (s, 4H); ^{13}C NMR ($CDCl_3$, 100 MHz) δ 18.5, 19.5, 127.4, 127.5, 130.2, 130.3, 132.7, 135.1, 137.7, 138.8, 139.6, 142.7, 192.6; FAB-MS (M + 1) 960.

Preparation of 3,3′,5,5′-Tetraphenylbimesityl: Tetraiodobimesityl **7** (2.22 g, 3.0 mmol), phenylboronic acid (2.90 g, 24.0 mmol), and $Pd(PPh_3)_4$ (0.69 g, 20 mol %) were introduced into an initially oven-dried and cooled (under N_2) pressure tube. To this mixture, dry toluene (15 mL) and saturated $NaHCO_3$ solution (15 mL) were added, and the resulting solution was bubbled with a nitrogen gas for 15 min. The pressure tube was sealed under nitrogen, and the reaction mixture was heated to 90−100 °C slowly and maintained at this temperature for 12 h with constant stirring. After this period, the reaction mixture was cooled and the contents were extracted with dichloromethane. A short pad filtration over silica gel using dichloromethane and hexane (1:19) yielded 3,3′,5,5′-tetraphenylbimesityl (1.25 g, 77%) as a colorless solid material: IR (KBr) cm^{-1} 3020, 2921, 1598, 1492, 1438; ^1H NMR (400 MHz, $CDCl_3$) δ 1.71 (s, 12H), 1.72 (s, 6H), 7.23 (m, 8H), 7.32 (m, 4H), 7.42 (m, 8H); ^{13}C NMR (100 MHz, $CDCl_3$) δ 18.3, 19.3, 126.2, 128.2, 129.5, 131.9, 132.4, 138.7, 140.0. 142.5.

Preparation of 3,3′,5,5′-Tetrakis(4-benzoylphenyl)bimesityl: A solution of $AlCl_3$ (1.44 g, 10.8 mmol) in CS_2 (20 mL) contained in a 50 mL two-necked round-bottom flask was cooled to 0 °C. Benzoylchloride (1.0 mL, 9.0 mmol) was slowly introduced into the flask at 10 °C. The solution of the 3,3′,5,5′-tetraphenylbimesityl (0.50 g, 0.9 mmol) in CS_2 (8 mL) was added to the reaction mixture dropwise over a period of 15 min at the same temperature. The resulting dark brown mixture was heated at reflux for 2.5 h. Subsequently, the contents were poured into an ice-cold 10% HCl solution. The organic material was extracted with ethyl acetate, washed with water, dried over anhyd Na_2SO_4, and concentrated. The pure product was obtained (0.70 g, 81%) after silica gel column chromatography using ethyl acetate/petroleum ether (1:9 → 1:4) as an eluent: IR (KBr) cm^{-1} 3053, 2923, 1722; ^1H NMR ($CDCl_3$, 400 MHz) δ 1.67 (s, 12H), 1.69 (s, 6H), 7.29 (d, J = 8.1 Hz, 8H), 7.44 (t, J = 7.4 Hz, 8H), 7.54 (t, J = 7.4 Hz, 4H), 7.80 (d, J = 7.1 Hz, 8H), 7.84 (d, J = 8.1 Hz, 8H); ^{13}C NMR ($CDCl_3$, 100 MHz) δ 18.4, 19.4, 128.3, 129.5, 130.0, 130.5, 131.7, 132.4, 132.6, 135.8, 137.6, 138.7, 139.4, 146.8, 196.6.

Representative Procedure for the Synthesis of Tetraphenylethene-Substituted Bimesitylene (5): A solution of 3,3′,5,5′-tetrakis(4-benzoylphenyl)bimesityl (0.44 g, 0.46 mmol) in THF (20 mL) was added slowly to the solution of diphenylmethyl lithium (generated from diphenylmethane (1.23 g, 7.34 mmol) and *n*-BuLi (4.0 mL of 1.6 M, 6.43 mmol) at −20 °C. The solution was slowly allowed to warm up to room temperature over a period of 3 h. The solution turned deep brown in color. After stirring for overnight at this temperature, the reaction mixture was quenched with water and the organic contents were extracted with ethyl acetate. The crude tetrahydroxy compound thus obtained was taken as it is to the next step without further purification. The crude product was later subjected to acid-catalyzed dehydration using dry toluene and a catalytic amount of PTS in a Dean−Stark apparatus. After reflux overnight, the solvent was evaporated to dryness. Silica gel column chromatography using chloroform and hexane mixture (1:4 → 1:1) afforded the required compound **5** as a colorless powder (yield 56%): IR (KBr) cm^{-1} 3053, 3023, 1598, 1493, 1442; ^1H NMR (400 MHz, $CDCl_3$) δ 1.50 (s, 12H), 1.58 (s, 6H), 6.83 (d, J = 8.0 Hz, 8H), 6.96 (br s, 24H), 6.98 (d, J = 8.0 Hz, 8H), 7.01 (m, 36H); ^{13}C NMR (100 MHz, $CDCl_3$) δ 18.2, 19.1, 126.3, 126.4, 127.4, 127.6, 128.8, 131.2, 131.35, 131.4, 131.8, 132.2, 138.6, 139.7, 140.6, 141.0, 141.1, 141.8, 143.5, 143.6, 143.8; FAB-MS 1558 (M + 1). Anal. Calcd for $C_{122}H_{94}$: C, 93.93; H, 6.07. Found: C, 93.50; H, 6.25.

3,3′-Bis-*p*-(2,2-diphenylvinyl)phenylbimesityl (1): This compound was synthesized starting from 3,3′-bis(4-formylphenyl-)bimesityl, **8**, following the above procedure used for the preparation of **5**: yield 62%; colorless powder; IR (KBr) cm^{-1} 3020, 2916, 1492, 1443; ^1H NMR (400 MHz, $CDCl_3$) δ 1.49 (s, 6H), 1.81 (s, 6H), 1.93 (s, 6H), 6.82−7.00 (m, 12H), 7.20−7.30 (m, 20H); ^{13}C NMR (100 MHz, $CDCl_3$) δ 17.8, 19.9, 20.8, 127.36, 127.40, 127.5, 128.1, 128.2, 128.6, 128.7, 129.1, 129.4, 130.3, 133.4, 134.0, 134.2, 135.4, 138.0, 139.5, 140.4, 140.5, 142.2, 143.5; FAB-MS 746 (M + 1). Anal. Calcd for $C_{58}H_{50}$: C, 93.25; H, 6.75. Found: C, 93.21; H, 6.72.

1,1-Diphenyl-2-biphenylethene-Substituted Bimesitylene (2): This compound was synthesized starting from 3,3′-bis(4(4′-formyl)biphenyl)bimesityl following the above procedure used for the preparation of **5**: yield 58%; colorless powder; IR (KBr) cm^{-1} 3053, 3021, 2919, 1493, 1443, 1376; ^1H NMR (300 MHz, $CDCl_3$) δ 1.66 (s, 6H), 1.96 (s, 6H), 2.05 (s, 6H), 7.02 (s, 2H), 7.06 (s, 2H), 7.11 (d, J = 8.2 Hz, 4H), 7.14−7.23 (m, 4H), 7.24−7.39 (m, 16H), 7.46 (d, J = 8.2 Hz, 4H), 7.58−7.64 (m, 4H); ^{13}C NMR (100 MHz, $CDCl_3$) δ 17.9, 19.9, 20.9, 126.4, 126.6, 127.4, 127.5, 127.6, 127.8, 128.2, 128.7, 128.8, 129.9, 130.0, 130.4, 133.5, 134.2, 134.4, 136.4, 138.1, 138.4, 139.0, 139.5, 140.4, 140.9, 142.6, 143.4; FAB-MS 898 (M^+). Anal. Calcd for $C_{71}H_{62}$: C, 93.17; H, 6.83. Found: C, 92.96; H, 6.68.

3,3′,5,5′-Tetrakis-*p*-(2,2-diphenylvinyl)phenylbimesityl (3): This compound was synthesized starting from 3,3′,5,5′-tetrakis(4-formylphenyl)bimesityl following the above procedure used for the preparation of **5**: yield 65%; colorless powder; IR (KBr) cm^{-1} 3053, 3021, 2919, 1597, 1493, 1443; ^1H NMR (400 MHz, $CDCl_3$) δ 1.50 (s, 18H), 6.80−6.90 (m, 6H), 6.92−7.00 (m, 10H), 7.14−7.35 (m, 46H); ^{13}C NMR (100 MHz, $CDCl_3$) δ 18.2, 19.3, 127.3, 127.4, 127.5, 128.1, 128.2, 128.6, 129.2, 129.4, 130.3, 131.8, 132.2, 135.4, 138.6, 139.6, 140.5, 140.9, 142.2, 143.5; FAB-MS 1255 (M + 1). Anal. Calcd for $C_{98}H_{78}$: C, 93.74; H, 6.26. Found: C, 93.73; H, 6.23.

1,1-Diphenyl-2-biphenylethene-Substituted Bimesitylene (4): This compound was synthesized starting from 3,3′,5,5′-tetrakis-(4(4′-formyl)biphenyl)bimesityl following the above procedure used for the preparation of **5**: yield 61%; colorless powder; IR (KBr) cm^{-1} 3052, 2920, 2852, 1597, 1493, 1442, 1389; ^1H NMR (400 MHz, $CDCl_3$) δ 1.65 (s, 12H), 1.68 (s, 6H), 6.94 (s, 4H), 7.03 (d, J = 8.0 Hz, 8H), 7.13−7.19 (m, 16H), 7.20−7.32 (m, 32H), 7.38 (d, J = 8.0 Hz, 8H), 7.45 (d, J = 8.0 Hz, 8H); ^{13}C NMR (100 MHz, $CDCl_3$) δ 18.4, 19.5, 126.3, 126.6, 127.0, 127.4, 127.5, 127.6, 127.7, 128.2, 128.7, 130.0, 130.4, 132.1, 132.5, 136.3, 138.3, 138.7, 138.9, 139.7, 140.4, 141.5, 142.6, 143.4; FAB-MS 1558 (M + 1). Anal. Calcd for $C_{122}H_{94}$: C, 93.93; H, 6.07. Found: C, 94.00; H, 6.00.

PL Quantum Yield Measurements:. Solution State For determination of fluorescence quantum yields, the solutions of bimesitylene-based OPVs **1**−**5** were prepared in cyclohexane (spectral grade) such that their absorbance at λ = 367 nm was ca. 0.025. These solutions were deaerated using nitrogen gas before their fluorescence was recorded at 298 K. The excitation wavelength was chosen as 367 nm for all the samples, and the emission in each case was recorded in a right angle mode. The quantum yield was calculated from the following relation:

$$\phi_u = \phi_s(A_s/A_u)(I_u/I_s)(\eta_u/\eta_s)^2$$

where the subscripts s and u refer to standard and unknown samples, A_u and A_s to absorbances of the sample and the

standard at the excitation wavelength, I_u and I_s to the integrated emission intensities (i.e., areas under the emission curves) of the sample and the standard, and η_u and η_s to the refractive indexes of the corresponding solutions (pure solvents are assumed). Anthracene was chosen as a reference for quantum yield determination, for which the reported quantum yield in ethanol is 0.27.[32]

Solid State. The films of compounds **1**−**5** were prepared on quartz plates (1 mm × 2 cm) by spin-coating of the solutions in 1,2-dichloroethane (10 mg/mL) at a constant rate of 300 rpm or by vacuum sublimation to a thickness of (1000 Å). The spin-coated quartz plates were dried in a vacuum oven, and the solid-state quantum efficiencies of the films were measured using an integrating sphere method.[33] The excitation source was 325 nm laser beam for all the samples.

Electrochemical Measurements. The cyclic voltammetry experiments were performed on an electrochemical analyzer, and the data were collected and analyzed using electrochemical analysis software. All experiments were carried out in a three-electrode compartment cell with Pt wire counter electrode, glassy carbon working electrode, and $Ag/AgNO_3$ (0.1 M) reference electrode at varying scan rates. The supporting electrolyte used was 0.1 M tetrabutylammoniumhexafluorophosphate solution in dry dichloromethane, and the cell containing the solution of the sample (1 mM) and the supporting electrolyte was purged with a nitrogen gas thoroughly before scanning for its oxidation and reduction properties. For each determination, the CV was run independently for ferrocene as a reference. The oxidation and reduction potentials of **1**−**5** were subsequently calculated from the average of anodic and cathodic peak potentials and were corrected according to the values observed for ferrocene oxidation. The HOMO and LUMO values were thus calculated with reference to the ferrocene oxidation potential by using the following general equations: $E_{HOMO} = E_{ox} + 4.8$ eV; $E_{LUMO} = E_{HOMO} - E_g^{opt}$.

(32) Melhuish, W. H. *J. Phys. Chem.* **1961**, *65*, 229.

(33) (a) de Mello, J. C.; Wittmann, H. F.; Friend, R. H. *Adv. Mater.* **1997**, *9*, 230. (b) Chiang, C.; Wu, M. F.; Dai, D. C.; Wen, Y. S.; Wang, J. K.; Chen, C. T. *Adv. Funct. Mater.* **2005**, *15*, 231.

Device Fabrication and Characterization of OLEDs. The multilayer OLEDs were fabricated by employing the OPVs **1**−**3** as emitting materials. The ITO-coated glass substrates with a sheet resistance of < 50 Ω/□ were cleaned sequentially in an ultrasonicator using acetone, detergent solution, deionized water, ethanol, and 2-propanol and then subjected to oxygen plasma and UV treatments.

Vacuum Deposition. Vacuum deposition of the organic materials such as NPB, **Bim-DPAB**, CBP, **1** or **2** or **3**, BCP, Alq_3, TPBI, LiF, and Al was carried out under a pressure of 10^{-6} Torr on top of etched ITO glass substrates sequentially. The rate of deposition for organic materials was maintained in the range 0.1−0.5 Å/s. The evaporation rate and thickness of the organic layers were monitored by a quartz oscillator. After the vacuum deposition, the devices were sealed in an inert atmosphere glovebox. EL spectra of the devices were obtained using a diode-array rapid analyzer system.

Electroluminescence Measurements. Current voltage and light intensity measurements were done on a source meter and an optical meter equipped with a silicon photodiode, respectively, The device was placed close to the photodiode such that all the forward light entered the photodiode. The effective size of the emitting diode was 4.0 mm^2, which is significantly smaller than the active area of the photodiode detector, a condition known as "under-filling", satisfying the measurement protocol.[34]

Acknowledgment. J.N.M. is thankful to the Department of Science and Technology (DST), India, for generous financial support. P.N. gratefully acknowledges the research fellowship from UGC−CSIR, India.

Supporting Information Available: ^1H and ^{13}C NMR characterization of the OPVs **1**−**5**, CV and DSC scans of the OPVs, and CIE coordinates obtained for the OLEDs. This material is available free of charge via the Internet at http://pubs.acs.org.

(34) Forrest, S. R.; Bradley, D. D. C.; Thompson, M. E. *Adv. Mater.* **2003**, *15*, 1043.